Journal of Intelligent & Robotic Systems (2023) 107:4
https://doi.org/10.1007/s10846-022-01797-9

SHORT PAPER

A Wire-driven Elastic Robotic Fish and its Design and CPG-Based Control

Xiaocun Liao[1,2] · Chao Zhou[1] · Jian Wang[1] · Junfeng Fan[1] · Zhuoliang Zhang[1,2]

Received: 27 April 2022 / Accepted: 16 December 2022 / Published online: 31 December 2022

Abstract

To simulate the complex and continuous undulation of fishtail in nature, the method of adopting the discrete Multi-Joint mechanism requires a certain number of degrees of freedom, which results in the complexities of mechanism and control necessarily. Compared with Multi-Joint, flexible tail is a better scheme due to continuum, robustness, and simpler control. Hence, this paper proposes a wire-driven elastic robotic fish with flexible tail, which simulates fish muscle through multi-wire drive and adopts a fishlike spine design based on elastic component. Due to these distinctive designs, our robotic fish not only realizes the compliant simulation of fishlike swimming gait, but also owns higher bionic degree. Further, the kinematics model and speed estimation model of the wire-driven elastic robotic fish are developed, and the error between the body wave and the desired fishlike swimming gait is further optimized so as to determine the appropriate parameters of central pattern generator. The results show that the optimized body wave of fishtail matches well with the desired fishlike swimming gait and the RMSE of the stable swimming speed between simulations and experiments is 0.045 m/s, which validates the proposed model and optimization method. Finally, the relationships between the frequency and swimming speed under small amplitude are explored, from which we find that amplitude has a greater impact on speed than frequency at high frequency, and the maximum swimming speed of about 0.54 m/s, i.e., 1.02 BL/s, is obtained.

Keywords Robotic fish · Wire-driven mode · Elastic component · Kinematics model · Body wave

1 Introduction

With the development and utilization of marine resources, underwater robot has become a novel tool for exploring ocean. However, compared with the fish in nature, man-made underwater robot is far inferior on performance, e.g., propulsive speed and efficiency. Some researches report that the propulsion efficiency and speed of some fish are as high as 90% and $110km/h$, respectively [1]. Inspired by the fish in nature, a growing number of researchers take interest in bionic robotic fish. In contrast to propeller-based underwater robot, robotic fish has the advantages of high propulsion efficiency and high maneuverability, which profits from fishlike swimming [2].

In recent years, the robotic fish based on wire-driven mode has also become a research hotspot due to its exquisite mechanical structure. Estarki et al. [3] presented a soft robotic fish with a wire-driven and soft body section, which could obtain an acceptable and trustable lateral motion at lower and higher frequencies. Zhong et al. [4] developed a robotic fish with active wire-driven body and compliant tail,

✉ Chao Zhou
chao.zhou@ia.ac.cn

Xiaocun Liao
liaoxiaocun2019@ia.ac.cn

Jian Wang
jianwang@ia.ac.cn

Junfeng Fan
junfeng.fan@ia.ac.cn

Zhuoliang Zhang
zhangzhuoliang2018@ia.ac.cn

[1] State Key Laboratory of Management and Control for Complex Systems, Institute of Automation, Chinese Academy of Sciences, No.95 Zhongguancun East Road, HaiDian District, Beijing, 100190, People's Republic of China

[2] School of Artificial Intelligence, University of Chinese Academy of Sciences, No.19 Yuquan Road, Shijingshan District, Beijing, 100049, People's Republic of China

whose maximum speed and average turning speed were 2.15 BL/s and 63°/s, respectively. Using vector propulsion, Li et al. [5] designed a wire-driven robotic fish with maximum speed of 0.35 BL/s, which could achieve two swimming modes similar to shark and dolphin. Lau et al. [6] designed a wire-driven robotic shark, which achieved the maximum speed of 0.22 BL/s and maximum body pitch angle of 17.3°.

Besides, continuum robotic fish, most of which are based on hydraulic pressure driving or artificial muscle, has developed rapidly. In contrast to conventional Multi-Joint robot fish with discrete rigid links, continuum robot fish can produce continuous bending motions by elastic deformation, which can achieve higher bionic degree. But, we have to notice that, owing to the limitations of fluidic pressure driving [7, 8] or artificial muscle [9], most of the existing continuum robotic fish only swim with low frequency, which means that the swimming speed is very low. As for the wire-driven robotic fish, many of which adopt the Multi-Joint based fishlike spine, are still with discontinuous body wave and complexity of mechanism essentially. Hence, it's desirable to explore an exquisite mechanism with the advantages of continuum and high swimming performance.

In addition, it is of great significance to design an effective control method to improve the swimming performance of the robotic fish. Generally, there are three basic motion control methods for bionic robotic fish, which are usually based on fitting body wave [10], dynamic model, or central pattern generator (CPG) [11]. The control method based on fitting body wave holds the advantages of simplicity and high efficiency. If the kinematics model of mechanism is obtained with difficulty, this method have the troubles in control. Since it is difficult to establish the accurate dynamic model of robotic fish, the applications of the model-based control method encounter some challenges. With regard to CPG, it has the advantages of few parameters, high efficiency and good stability, and has been widely used in robotic fish's control. Based on Hopf Oscillators, Yang et al. [12] proposed a CPG network topology model for amphibious robotic fish to obtain various motion gaits. Cao et al. [13] constructed a CPG-based controller for manta ray robot, and the CPG parameters were optimized so as to obtain better bionic effect. By integrating CPG controller and Lagrangian dynamic model, Wang et al. [14] presented a self-propelled, multimodal ostraciiform robotic fish. Using CPG controller, a RBF neural network and an adaptive algorithm, Zhang et al. achieved the pitch control of a robotic fish with three degree-of-freedom(DOF) pectoral fins, wire-driven flexible body and a passive caudal fin [15].

In many previous studies, CPG parameters were determined manually according to experience, indicating that it's inefficient to tune too many CPG parameters. In some previous studies, several methods were proposed to refine CPG parameter. Jeong et al. [16] utilized Particle Swarm Optimization (PSO) [17] to refine the CPG parameters of robotic fish so as to obtain fishlike swimming. Based on PSO, Wang et al. [18] proposed a optimization method for CPG parameters, and realized the smooth control signal and high swimming speed of robotic fish. By using PSO to optimize the CPG parameters for pursuing high propulsive efficiency and forward speed, Wang et al. [19] presented a four-joint robotic fish with the maximum average speed of 0.53 m/s. Yuan et al. [20] explored the effects of the oscillator phase differences of CPG on the swimming performance including steady forward velocity, head stability as well as energy-efficiency, and proposed the optimization method of the CPG parameters based on the genetic algorithm (GA) to improve the swimming performance. To maximize the speed of an amphibious snake robot, a gradient-free optimization algorithm was applied to tune the CPG parameters including phase lag, oscillation amplitude [21]. An on-line searching method of the CPG parameters, based on the GA, was implemented improve swimming speed and energy efficiency for a biomimetic fin propulsor [22]. Besides, Tong et al. [23] proposed a reinforcement-learning-based online optimization of CPG parameters to improve the swimming speed and swimming stability.

The main purpose of this paper is to develop an untethered robotic fish with the advantages of continuum and high swimming performance, which makes better use of the merits of wire-driven mode. The main contributions of this paper are as follows:

- Based on our previous work in [24], we implement the waterproof design as well as size optimization, and successful develop an untethered wire-drive elastic robotic fish, which can swim freely.
- An improved kinematic model is proposed in this paper, which can calculate the positions of any point of fishtail. Besides, a speed estimation model is also derived to explore swimming performance.
- In response to the mechanical coupling resulted from dual-wire driven mode, the PSO-based optimization for the CPG parameters is presented to obtain fishlike swimming gait based on the improved kinematic model.
- Plenty of simulations and free-swimming experiments are conducted to validate the feasibility of the bionic mechanism and the proposed algorithm.

The remainder of this paper is organized as follows. Section 2 depicts the mechatronic design of robotic fish and CPG-based controller, and Section 3 presents the kinematics model and speed estimation model. The CPG parameter optimization is presented in Section 4. Section 5

presents simulations and experiments. Finally, conclusions and future works are summarized in Section 6.

2 Overview of Wire-driven Elastic Robotic Fish

2.1 Mechatronic Design

Figure 1 shows the overview design of our novel wire-driven elastic robotic fish, which is composed of a rigid head, a wire-driven elastic tail and a rigid caudal fin. Its size and mass are $530(L) \times 106(W) \times 150(H)\ mm^3$ and 3.3 kg, respectively. The fish head is divided into a control cabin, where control circuit and battery are equipped, and a drive cabin, where two servomotors, drive shafts and reels are mounted.

Next, we focus on the design of bionic fishtail. For the existing wire-driven robotic fish, most of which adopt fishlike spine based on Multi-joint [4, 5], are with the discontinuous body wave and complexity of mechanism essentially. To overcome this hurdle, the elastic component, i.e., spring-steel-sheet, is adopted as fishlike elastic spine of our robotic fish, and owns trapezoidal shape, which can simulate the convergent spine of fish well. The whole fishtail is continuum, indicating that our robotic fish is with continuous body wave and higher bionic degree.

Further, five oval metal plates I - V are sequentially mounted on the elastic spine and fixed by several clamps. The size of these five oval metal plates I - V decrease in turn, which can simulate the convergent fishtail in nature. The oval metal plates I - II and IV are only used to support fish skin, so as to maintain the shape of fishtail during swimming. The remaining two oval plates serve as the power mechanism of tail. Concretely, based on two pairs of inelastic wires, the output torques of two servomotors are transmitted to the oval plates III and V of fishtail, which can realize fishtail-like swing. In contrast to some existing wire-driven robotic fish with one motor [3, 4], our robotic fish are driven by two servomotors, meaning that some complex shapes of fishtail, such as C-shape and S-shape, can be achieved [24]. The wire-driven elastic tail of robotic fish is sealed by silicone rubber, and the tuna-inspired caudal fin is connected to the end of the elastic spine. In fact, the connection point between tail and caudal fin can be regarded as a passive flexible joint (PF-Joint), which is capable of improving motion performance of robotic fish in some cases [25]. We ignore the effect of the PF-Joint due the relatively short length of PF-Joint in this paper.

The control system configuration of the robotic fish, shown in Fig. 2, is composed of four components, i.e., power unit, control unit, actuator unit, communication unit and sensor unit. The power unit includes battery and DC/DC converters, providing voltage for other electronic components. The control unit is based on the embedded chip of STM32F407, and the Real Time Operating System of FreeRTOS is adopted to ensure the quick response to control and communication. The actuator unit consists of two servomotors, which are actuated by the Pulse Width Modulation (PWM) of the control unit. The communication unit, including RF200 and Bluetooth, is applied to send and receive data with upper computer. Besides, the attitude information (including roll, pitch, and yaw) is obtained by the Inertial Measurement Unit (IMU, MPU6050).

2.2 CPG Controller

Since Ijspeert's CPG model [26] owns the advantages of few parameters and explicit meaning of parameters, it is suitable

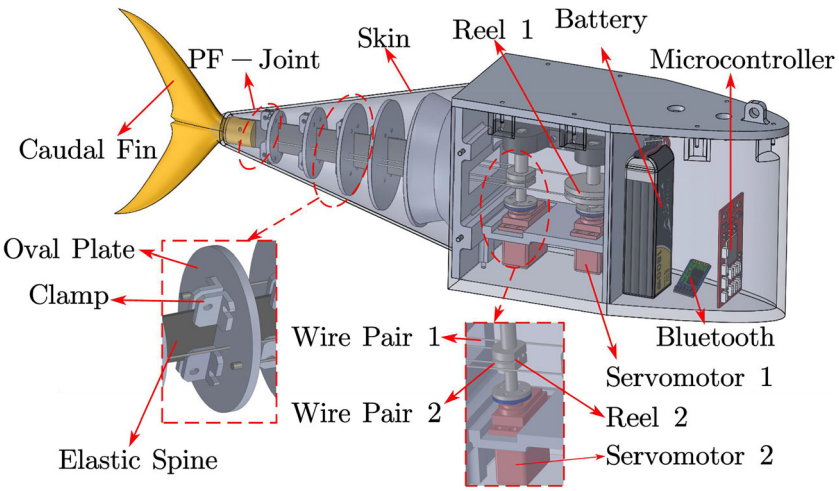

Fig. 1 Overview design of the novel wire-driven elastic robotic fish

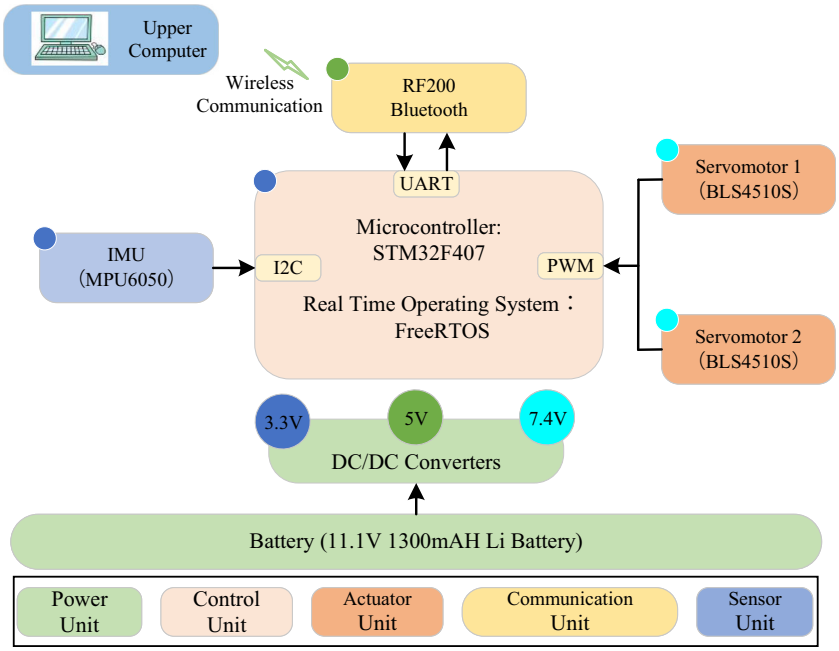

Fig. 2 Control system configuration of robotic fish

for the robotic fish. The Ijspeert's oscillator is as follows:

$$\begin{cases} \dot{\xi}_i = 2\pi v_i + \sum\limits_{j,j\neq i} r_i \omega_{ij} \sin(\xi_j - \xi_i - \varphi_{ij}) \\ \ddot{r}_i = \alpha_i(\frac{\alpha_i}{4}(R_i - r_i) - \dot{r}_i) \\ \Theta_i = r_i \cos(\xi_i) + b_i \end{cases}, \tag{1}$$

where ξ_i and r_i are the state variables, representing the phase and amplitude of the i-th oscillator, respectively; v_i and R_i determine convergence frequency and amplitude, respectively, and α_i that is positive constant determines the convergence speed. The coupling between the i-th and j-th oscillator is determined by the weight ω_{ij} and phase deviation φ_{ij}. b_i and Θ_i are the offset and final output signal of the i-th oscillator, respectively. Since our robotic fish is driven by two servomotors, a CPG network with two Ijspeert's oscillators is constructed. The sketch of CPG-based control for our robotic fish is shown in Fig. 3.

3 Kinematics Model and Speed Estimation

3.1 Kinematics Model

As shown in Fig. 4, the base coordinate systems, $C_0 = \{O_0 - X_0Y_0\}$, is defined. The origin O_0 is located at the center of oval metal plate I, the axis X_0 is always parallel to the initial body axis and points to the end of tail, and the axis Y_0 is determined according to the right-hand rule. Similarly, two relative coordinate systems $C_1 = \{O_1 - X_1Y_1\}$ and $C_2 = \{O_2 - X_2Y_2\}$ are defined. It is worth noting that the origin O_1 and O_2 are located at the center of oval metal plate III and V, respectively, and the axis X_1 and X_2 always remain tangent to the body axis. For convenience, the fishtail of the oval metal plate I to III and III to V are referred to as the flexible link $\hat{L}_1$ and $\hat{L}_2$, respectively. Let denote $\hat{l}_1$ and $\hat{l}_2$ as the length of the flexible link $\hat{L}_1$ and $\hat{L}_2$, respectively. The caudal fin is rigid and defined as L_3. l_3 represents the length of L_3.

As can be seen from Fig. 4, when two servomotors of robotic fish are driven, the wire-driven elastic fishtail swing like the fishtail in nature and the two flexible links $\hat{L}_1$ and $\hat{L}_2$ bend periodically. Assuming that the shapes of two flexible links are all arcs after bending. The central angle $\beta_i (i = 1, 2)$ of the flexible link $\hat{L}_i$ is defined as positive when bending to right.

To get the body wave function, the mechanical coupling of the mechanism need to be solved firstly. According to the

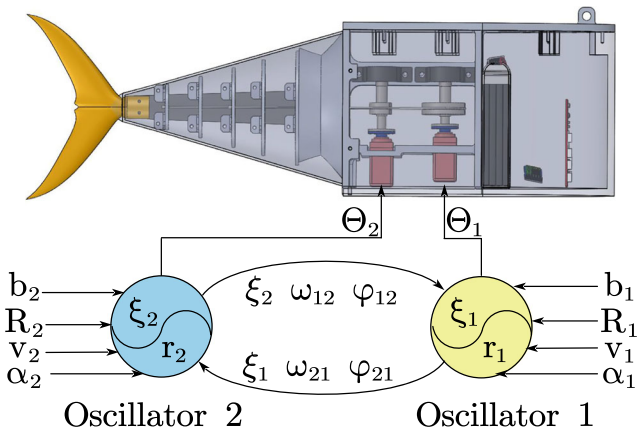

Fig. 3 The sketch of CPG-based control for our robotic fish

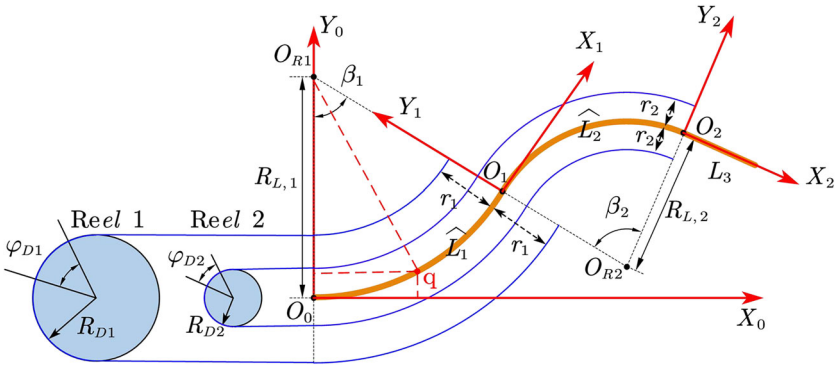

Fig. 4 Schematic illustration of coordinate systems and notations

Fig. 4, the changes of two wire pairs can be expressed as follows:

$$\begin{aligned} \Delta l_1 &= R_{D_1}\varphi_{D_1} = r_1\beta_1 \\ \Delta l_2 &= R_{D_2}\varphi_{D_2} = r_2\beta_1 + r_2\beta_2, \end{aligned} \tag{2}$$

where Δl_1 and Δl_2 are the changes for wire pair 1 and 2, respectively; R_{D_1} and R_{D_2} are radii for the 1st and 2nd reel, respectively; r_1 and r_2 are distances between wire pair 1, 2 and the body axis of fishtail, respectively; φ_{D_1} and φ_{D_2} are rotation angles of the 1st and 2nd reel, and equal to Θ_1 and Θ_2 of CPG output, respectively. Then, we can obtain:

$$\beta_1 = \frac{R_{D_1}\varphi_{D_1}}{r_1}, \tag{3}$$

$$\beta_2 = \frac{R_{D_2}\varphi_{D_2}}{r_2} - \beta_1, \tag{4}$$

$$R_{L,1} = \frac{\hat{l_1}}{\beta_1}, \tag{5}$$

$$R_{L,2} = \frac{\hat{l_2}}{\beta_2}, \tag{6}$$

where $R_{L,1}$ and $R_{L,2}$ are the arc radii of the flexible link $\hat{L_1}$ and $\hat{L_2}$ after bending, respectively. Specially, if β_i $(i = 1, 2)$ is equal to zero, $R_{L,i}$ is infinite, which is a singular case.

Further, the generalized coordinate q, which is along the body axis, is defined. Note that the generalized coordinate q of the origin O_0 is 0. Let denote ${}^i x(q,t)$ and ${}^i y(q,t)$ as the components of the position of the point q on the axis X_i and Y_i, respectively. ${}^i\boldsymbol{R}_j$ and ${}^i\boldsymbol{P}_j$ represent the rotating transformation matrix and position vector of coordinate system C_j with respect to C_i, respectively. Based on the aforementioned arc assumption, the body wave functions of the wire-driven elastic fishtail with respect to C_0, that is, $x(q,t)$ and $y(q,t)$, can be derived.

- If $0 \le q \le \hat{l_1}$,

$$\begin{bmatrix} x(q,t) \\ y(q,t) \end{bmatrix} = \begin{bmatrix} R_{L,1}\sin(q\beta_1/\hat{l_1}) \\ R_{L,1}\left[1-\cos(q\beta_1/\hat{l_1})\right] \end{bmatrix}. \tag{7}$$

- If $\hat{l_1} < q \le \hat{l_1} + \hat{l_2}$,

$$\begin{bmatrix} x(q,t) \\ y(q,t) \end{bmatrix} = {}^0\boldsymbol{R}_1 \begin{bmatrix} {}^1x(q,t) \\ {}^1y(q,t) \end{bmatrix} + {}^0\boldsymbol{P}_1, \tag{8}$$

where,

$$\begin{bmatrix} {}^1x(q,t) \\ {}^1y(q,t) \end{bmatrix} = \begin{bmatrix} R_{L,2}sin((q-\hat{l_1})\beta_2/\hat{l_2}) \\ R_{L,2}\left[1-\cos((q-\hat{l_1})\beta_2/\hat{l_2})\right] \end{bmatrix}, \tag{9}$$

$${}^0\boldsymbol{R}_1 = \begin{bmatrix} \cos\beta_1 & -sin\beta_1 \\ sin\beta_1 & \cos\beta_1 \end{bmatrix}, \tag{10}$$

$${}^0\boldsymbol{P}_1 = \begin{bmatrix} x(\hat{l_1},t) \\ y(\hat{l_1},t) \end{bmatrix} = \begin{bmatrix} R_{L,1}sin(\beta_1) \\ R_{L,1}\left[1-\cos(\beta_1)\right] \end{bmatrix}. \tag{11}$$

- If $\hat{l_1} + \hat{l_2} < q \le \hat{l_1} + \hat{l_2} + l_3$,

$$\begin{bmatrix} x(q,t) \\ y(q,t) \end{bmatrix} = {}^0\boldsymbol{R}_2 \begin{bmatrix} {}^2x(q,t) \\ {}^2y(q,t) \end{bmatrix} + {}^0\boldsymbol{P}_2, \tag{12}$$

where,

$$\begin{bmatrix} {}^2x(q,t) \\ {}^2y(q,t) \end{bmatrix} = \begin{bmatrix} q-\hat{l_1}-\hat{l_2} \\ 0 \end{bmatrix}, \tag{13}$$

$${}^0\boldsymbol{R}_2 = \begin{bmatrix} \cos(\beta_1+\beta_2) & -sin(\beta_1+\beta_2) \\ sin(\beta_1+\beta_2) & \cos(\beta_1+\beta_2) \end{bmatrix}, \tag{14}$$

$${}^0\boldsymbol{P}_2 = \begin{bmatrix} x(\hat{l_1}+\hat{l_2},t) \\ y(\hat{l_1}+\hat{l_2},t) \end{bmatrix} = {}^0\boldsymbol{R}_1 \begin{bmatrix} {}^1x(\hat{l_1}+\hat{l_2},t) \\ {}^1y(\hat{l_1}+\hat{l_2},t) \end{bmatrix} + {}^0\boldsymbol{P}_1. \tag{15}$$

According to the Eqs. 7, 8 and 12, the swing rhythmic of fishtail, that is, the positions of any point on fishtail with respect to C_0, can be obtained.

3.2 Swimming Speed Estimation

To analyze the swimming performance of our robotic fish, it's necessary to develop an accurate model for speed estimation, which provides an effective tool for speed optimization and mechanism improvement. Note that, compared with the body length of our robotic fish, its lateral movement are relatively small. Therefore, the Lighthill's

model based on the large amplitude elongated body theory is feasible for our robotic fish.

According to the Lighthill's model [27], the mean thrust F_T and drag force F_D can be obtain and expressed as follows:

$$F_T = \left[\frac{\rho A(L_T)}{2}\left\{\overline{\left\{\frac{\partial y(q,t)}{\partial t}\right\}^2} - U_c^2\overline{\left\{\frac{\partial y(q,t)}{\partial q}\right\}^2}\right\}\right]\Bigg|_{q=L_T,} \tag{16}$$

$$F_D = \frac{1}{2}C_D\rho U_c^2 S_c, \tag{17}$$

where L_T, representing the tail tip, is equal to $\hat{l_1}+\hat{l_2}+l_3$ in this paper; ρ is the fluid density; U_c is the stable speed; C_D represents the drag coefficient; S_c and $A(L_T)$ are the total surface area and the area of the cross section of the tail tip, respectively. Assuming that the mean thrust is balanced by drag force when the robotic fish cruise with uniform speed. Then, we can derive the stable speed U_c.

$$U_c = \left[\frac{\rho A(L_T)\overline{\left\{\frac{\partial y(q,t)}{\partial t}\right\}^2}}{\rho C_D S_c + \rho A(L_T)\overline{\left\{\frac{\partial y(q,t)}{\partial q}\right\}^2}}\right]^{\frac{1}{2}}\Bigg|_{q=L_T} \tag{18}$$

According to the Eq. 12, the partial derivative of $y(q,t)$ can be derived as follows:

$$\frac{\partial y(q,t)}{\partial q} = sin(\beta_1+\beta_2) \tag{19}$$

$$\frac{\partial y(q,t)}{\partial t} = \frac{\partial y(q,t)}{\partial \beta_1}\dot{\beta_1} + \frac{\partial y(q,t)}{\partial \beta_2}\dot{\beta_2} \tag{20}$$

where $\dot{\beta_1}$ and $\dot{\beta_2}$ are the bending angle velocity of the flexible link $\hat{L_1}$ and $\hat{L_2}$, respectively, and according to the Eqs. 3 and 4, they can be expressed by

$$\dot{\beta_1} = \frac{R_{D_1}\dot{\varphi_{D_1}}}{r_1}, \tag{21}$$

$$\dot{\beta_2} = \frac{R_{D_2}\dot{\varphi_{D_2}}}{r_2} - \dot{\beta_1}, \tag{22}$$

where $\dot{\varphi_{D_1}}$ and $\dot{\varphi_{D_2}}$ are the angular velocity of the servomotor 1 and 2, respectively. Combining the Eqs. 18, 19, 20, 21 and 22, the stable speed U_c can be estimated.

4 Optimization of CPG Parameter

4.1 CPG Parameter Optimization

When designing and controlling our robotic fish, we avail the theoretical studies of how fish swim efficiently, as much as possible. Inspired by the fish with Body and/or Caudal Fin (BCF) swimming mode, Lighthill proposed that the body wave of a swimming fish is a travelling wave, which can be expressed by

$$y_{body}(q,t) = (c_1 q + c_2 q^2)sin(kq+\omega t), \tag{23}$$

where c_1 and c_2 are the linear and quadratic coefficient of wave amplitude envelope, respectively, and ω is the body wave frequency. k is the body wave number, which can change swimming modality from oscillatory swimming to undulatory swimming. Based on Lighthill's model, some wave model for fish were proposed, e.g., Alvarado's model [28].

In this paper, the Lighthill's body wave model is adopted to generate the fishlike swimming gait. To achieve the fishlike swimming, the primary task of this paper is to determine the appropriate CPG parameters so as to generate the rhythmic signal and further make the swing rhythmic of fishtail close to any given body wave. However, compared with some existing wire-driven robotic fish [3, 4], our robotic fish has mechanical coupling, and the inverse kinematics model is complicated, which results in difficulty in determining CPG parameters. With the consideration of this, based on the proposed kinematics model, the PSO-based optimization for the CPG parameters is presented to minimize the error between the swing rhythmic of wire-driven elastic fishtail and the desired body wave. The optimization goal of fitting body wave is defined as follows:

$$loss = \min_{\lambda}\int_{t_s}^{t_o}\|e(t)\|dt, \tag{24}$$

where

$$e(t) = \sum_{i=1}^{2}\|y_{body}(q_i,t) - y(q_i,t)\|, \tag{25}$$

λ is the collection of optimized CPG parameters; $y_{body}(x,t)$ with respect to C_0 is desired body wave determined by the Eq. 23, and $y(x,t)$ is value derived by the kinematics model. q_1 and q_2 are the generalized coordinates of the origin O_1 and O_2, respectively. Note that the output signals of the CPG controller have stabilized between t_s and t_o in this optimization.

For simplicity, the optimizations based on $loss$ is referred to as point optimization, which is analyzed under the assumption that the maximum output torque of the servomotor is infinite, that is, the servomotor can reach any given rotation angle. The CPG optimized by the point optimization only determines the expected rotation angle of two servomotor, and the responses of CPG depend on the performance of the servomotor when there is some turbulence in water. According to the Eqs. 24 and 25, it's obvious that the physical meaning of the point optimization is to minimize the error between the actual positions of two active joints of fishtail and joint positions of desired body wave during the optimization cycle. Obviously, the smaller

the optimization goal $loss$ is, the better the optimization effect is. In other words, based on the point optimization, we can build the mapping mechanism between the fishlike swimming gait and CPG parameters. Note that, in the practical applications, the desired body wave is determined by the upper tasks, e.g., obstacle avoidance, target tracking. For example, robotic fish need to perform turning motion, if there is an obstacle in front of it. The decision making system of robotic fish can determine a desired body wave, and then the CPG parameters need to be tuned so as to make the swing rhythm of fishtail close to this desired body wave.

Note that the CPG model constructed in this paper contains 10 parameters. v_i can be determined by swing period T, and α_i is set to 20. Since the straight motion is taken into consideration, b_i $(i = 1, 2)$ is determined as 0. The remaining 6 parameters, including ω_{ij}, φ_{ij} and R_i $(i, j = 1, 2; j \neq i)$, need to be optimized to generate desired output signals. Given that point optimization is nonlinear optimization problem, Particle Swarm Optimization (PSO) is adopted in this paper.

4.2 Particle Swarm Optimization

In each iteration of PSO, the i-th particle updates its velocity $\vartheta_{i,d}$ and position $\chi_{i,d}$ based on the individual optimal solution $p_{i,d}$ and global optimal solution $p_{g,d}$.

$$\begin{aligned}\vartheta_{i,d} &= c_w\vartheta_{i,d} + c_{f,1}r_{f,1}(p_{i,d} - \chi_{i,d}) \\ &\quad + c_{f,2}r_{f,2}(p_{g,d} - \chi_{i,d}) \qquad (26)\\ \chi_{i,d} &= \chi_{i,d} + \vartheta_{i,d} \qquad (27)\end{aligned}$$

The symbol c_w is the weight coefficient, $c_{f,1}$ and $c_{f,2}$ are learning factors, $r_{f,1}$ and $r_{f,2}$ are random values, and the subscript d represents the dimension of each particle, that is, the number of optimization variables in optimization problem.

Given the optimization efficiency and actual drive effect, the constraints on the optimized parameters, i.e., $\omega_{ij} \in [-10, 10]$, $\varphi_{ij} \in [-\pi, \pi]$ (rad) and $R_i \in [-\pi/2, \pi/2]$ (rad), $(i, j = 1, 2; j \neq i)$, are set.

Based on the above analysis, for any given fishlike swimming gait, the CPG parameters can be refined efficiently based on Eq. 24 and PSO.

5 Simulations and Experiments

5.1 Experimental Platform

Figure 5 shows experimental platform for our wire-driven elastic robotic fish. The Bluetooth-based communication between upper computer and robotic fish is applied to realize the sending and receiving of commands and data. A global camera, which can capture the surroundings and the motion of robotic fish during experiments, is hung over the pool.

5.2 Simulations of CPG Parameter Optimization

In this study, we use the body wave with $\omega = 2\pi$, $c_1 = 0.15$, $c_2 = 1$, $k = 8$, meaning that $v_i = \omega/(2\pi) = 1\ Hz$ $(i = 1, 2)$. The parameters of body wave are selected according to the empirical values and slightly modified [1]. Based on the aforementioned optimization algorithm, the desired CPG parameters can be obtained.

The convergence curve of $loss$ is plotted in Fig. 6(a), from which, we find that point optimization can obtain relatively good solutions (4.6067) within 10 iterations, indicating that the optimization algorithm we proposed is fast on calculation. Figure 6(b) shows the convergence tendency of 6 optimized CPG parameters based on point optimization. Since the optimized CPG parameters are randomly set at the initial moment, violent oscillations for CPG parameters occur in the first 10 iterations. As the iteration progresses, the better solutions are found and the curve tendency becomes more stable. The red dotted line

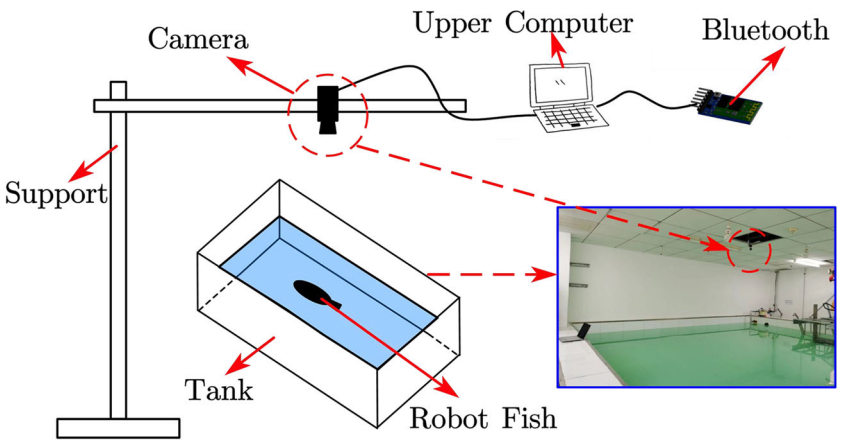

Fig. 5 Experimental platform for the wire-driven robotic fish

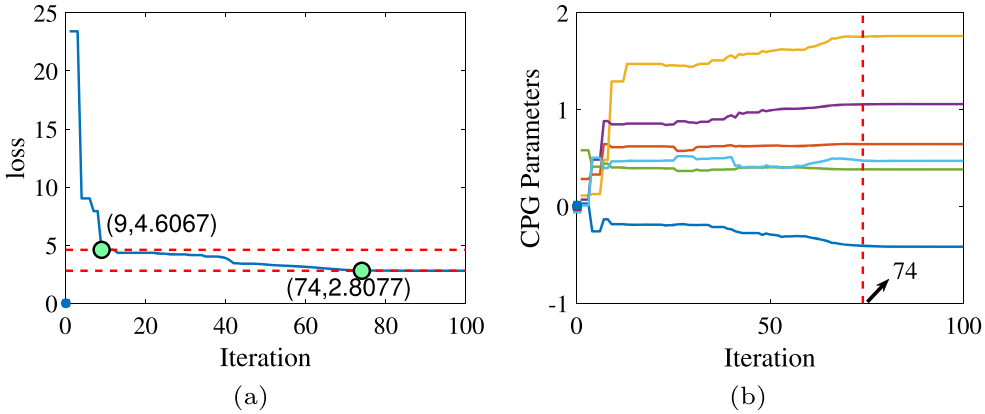

Fig. 6 (a) The convergence curve for $loss$; (b) The convergence curves for CPG parameters

in Fig. 6(b) indicates that the optimal solution has been obtained. The convergence values of CPG parameters are listed in Table 1.

In order to describe the motion of fishtail, two swing angles, $\theta_i = \angle(O_0O_i, O_0X_0)$ $(i = 1, 2)$, are defined. $\bar{\theta}_i$ is defined as the expected value of θ_i and can be derived from Eq. 23. The CPG parameters obtained by aforementioned optimization are applied to CPG controller of our robotic fish. Figure 7(a) reveals the optimized outputs of the CPG controller. Based on kinematics model, two swing angles of fishtail are obtained, as shown in Fig. 7(c). Comparing Fig. 7(b) with (c), we can find that θ_i $(i = 1, 2)$ match well with $\bar{\theta}_i$ and two swing angles θ_i are sinusoidal. In addition, the Root Mean Squared Error (RMSE) of θ_1 and θ_2 are 1.7165° and 1.2817°, respectively, which also validates the fishtail-like swing of our robotic fish. Figure 7(d) depicts the results of the evolution of fishtail in one period. As we expect, the body wave of fishtail matches well with the expected value and the ends of the flexible link $\hat{L}_1$ and $\hat{L}_2$ (represented by dots and squares, respectively) are located on the desired body wave at any time, indicating that the goal of point optimization has achieved.

5.3 Experiments of parameter optimization

Based on point optimization, we can make the wire-driven elastic fishtail undulate according to the desired fishlike swimming gait. More importantly, we hope to realize the stable fishlike swimming of robotic fish by the proposed optimization algorithm. Hence, the optimized CPG parameters are further applied to the control of our wire-driven elastic robotic fish so as to further investigate the swimming performance.

The curve of frequency and swimming speed are shown in Fig. 8(a), from which, we find that the higher the frequency of robotic fish is, the greater the speed is, which is consistent with the real law. Figure 8(b) shows the snapshot sequences of movement for our wire-driven elastic robotic fish with the frequency of 3 Hz, and the maximum stable swimming speed of about 0.39 m/s, i.e., 0.74 BL/s, is obtained. In Fig. 8(b), the reason why the robotic fish turns is attributed to the disturbance of water waves. From Figs. 7(d) and 8, it can be concluded that point optimization not only is capable of controlling the undulation of wire-driven elastic fishtail according to the desired swimming gait, but also achieves the stable swimming of robotic fish.

5.4 Stable Swimming Speed

In the aforementioned experiments, we aim to explore whether the proposed optimization algorithm can control fishtail to undulate according to the desired rhythmic, and whether robotic fish can achieve stable swimming. On the basis of stable swimming, we further desire that our robotic fish can achieve higher swimming speed. Hence, the relationships between swing amplitude, frequency and swimming speed of robotic fish are explored, which can provide the experimental basis for improvements on mechanism design.

We measure the stable swimming speed of robotic fish under different swing amplitudes and frequencies. The frequency is set to $f = (k * 0.2 + 1)$ Hz, $k = 0, 1, ..., 10$, and amplitude is chosen from $\{4, 4.5, 6.5, 8, 9\}$ cm. It is worth mentioning that the remaining CPG parameters are determined by point optimization and tabulated in Table 1. Furthermore, based on the speed estimation model, the

Table 1 The convergence values of CPG parameters

Parameters (λ)	ω_{12}	ω_{21}	$\varphi_{12}(rad)$	$\varphi_{21}(rad)$	$R_1(rad)$	$R_2(rad)$
value	-0.41	0.64	1.76	1.06	0.38	0.47

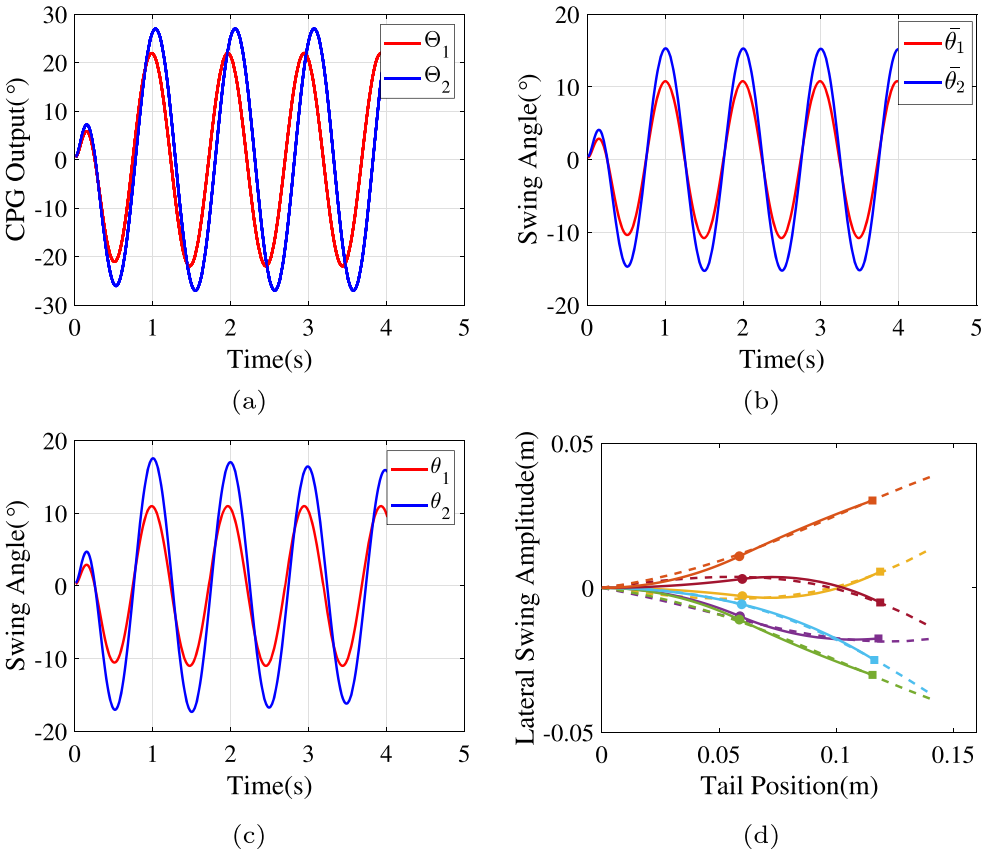

Fig. 7 (a) is the CPG outputs obtained by point optimization; (b) and (c) show the expected and predicted swing angle, respectively; Evolution for fishtail in one period is depicted in (d); Solid lines represent the fishtail's position obtained by kinematics model; Dotted lines represent the desired body wave; The circles and squares represent the ends of the flexible link $\hat{L}_1$ and $\hat{L}_2$, respectively

estimated stable swimming speed can be obtained. As can be seen from Fig. 9, it's clear that the higher the frequency and amplitude of robotic fish are, the greater the speed is, which is in accord with objective law. Besides, comparing Fig. 9(a) with (b), we can find that the stable swimming speed of simulation matches well with experiments, and the RMSE of the stable swimming speed between simulations and experiments is 0.045 m/s, which validates the accuracy of speed estimation model.

In robotic fish, swimming number (Sw), representing the distance fish moved per tail beat, is a widely used indicator to evaluate the propulsion performance, and can be expressed by $Sw = U/fL$ [29], where U is the stable swimming speed, f represents the tail-beating frequency, and L is the body length. For fish, the swimming number Sw is about 0.6, indicating that it is generally about 0.6 for very high performances in robotic fish [29]. The Sw of our robotic fish under different amplitudes and frequency are depicted in Fig. 10. The RMSE of Sw between simulations and experiments is 0.0416 and the speed estimation model is verified again. Besides, we can find that Sw also increases with the increase of amplitude, and the maximum experimental Sw is about 0.33, when the frequency and amplitude are 1 Hz and 9 cm, respectively.

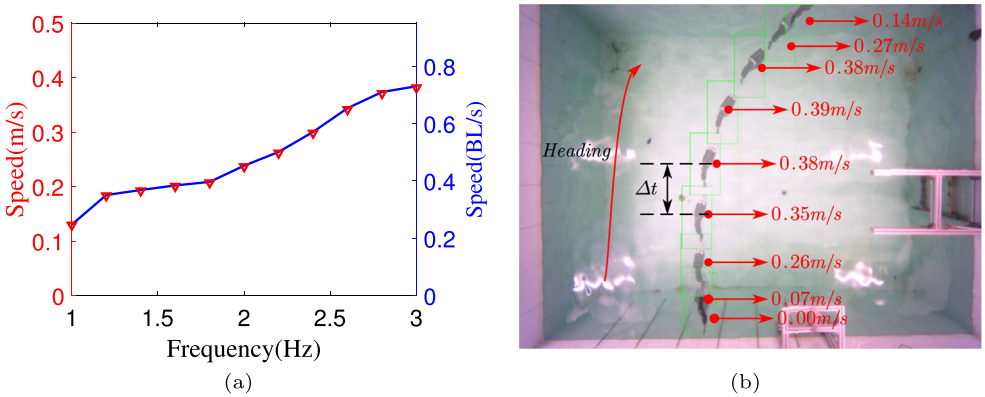

Fig. 8 (a) The curve of stable swimming speed and frequency; (b) Snapshot sequences of our wire-driven elastic robotic fish with the frequency of 3 Hz; The swimming speed in (b) is the average speed within 1s, and the time span Δt is 1.7s

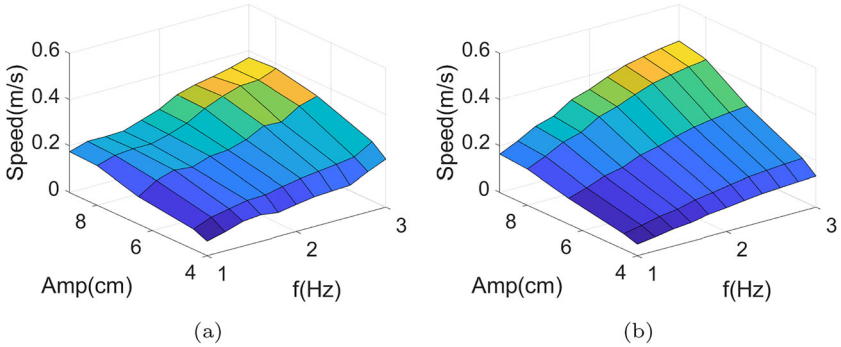

Fig. 9 The curve for stable swimming speed, frequency and amplitude; (a) Experiment; (b) Simulation; Note that the intersection points of grid-line represent the experimental data in (a)

Despite the difference in Sw between our robotic fish and fish, compared with some existing wire-driven robotic fish, *e.g.*, Lau's wire-driven robotic fish(0.11) [6] and Liu's continuum robotic dolphin(0.176) [30], our robotic fish are better in Sw.

Since the performance of servomotors is limited, we choose the maximum frequency of 3 Hz in the previous experiment. That is, the motion on large amplitude and high frequency can't be achieved. In order to further investigate more fast swimming speed of our wire-driven elastic robotic fish, the lower amplitude of 5 cm is chosen and the frequency is further increased. As shown in Fig. 11, when the frequency is less than 6.5 Hz, the speed and frequency are positively correlated. When the frequency is 6.5 Hz, the maximum swimming speed of 0.54 m/s, i.e., 1.02 BL/s, is obtained. According to the observations of the fishtail, the swing amplitude decreases obviously when the frequency is over 5 Hz, meaning that the servomotor can't approach the given angle obtained by CPG in real time due to the performance limitation of servomotor. It's also reflected by the experimental results that the speed growth is significantly slower with the increase of frequency when the frequency is over 5 Hz, and the speed and frequency are negatively correlated when the frequency is greater than 6.5 Hz. This finding indicates that amplitude has a greater impact on speed than frequency at high frequency.

The speed comparisons between our robot fish and the existing wire-driven robot fishes are presented in Table 2, from which, we find that the maximum swimming speed of most of the existing wire-driven robot fish is less than 1 BL/s, and our wire-driven elastic robotic fish obtains relatively high swimming speed of 1.02 BL/s.

5.5 Conclusions for Experiments

Based on the experiments and discussions above, the conclusions can be drawn as follows:

- Point optimization are effective and can find relatively good solutions within 10 iterations, indicating that the optimization algorithm we proposed is fast on calculation. Base on this method, our robotic fish has high swimming stability, and bionic fishtail can undulate according to the desired fishlike swimming gait.
- Our wire-driven elastic fishtail-like propeller holds the merits of contimuum, high frequency swimming and high bionic degree, which can be well applied to simulate tail of fish in nature.
- For our robotic fish, when the frequency is between 1 Hz and 3 Hz, the fact is that the higher the frequency and amplitude of the robotic fish are, the greater the speed is.

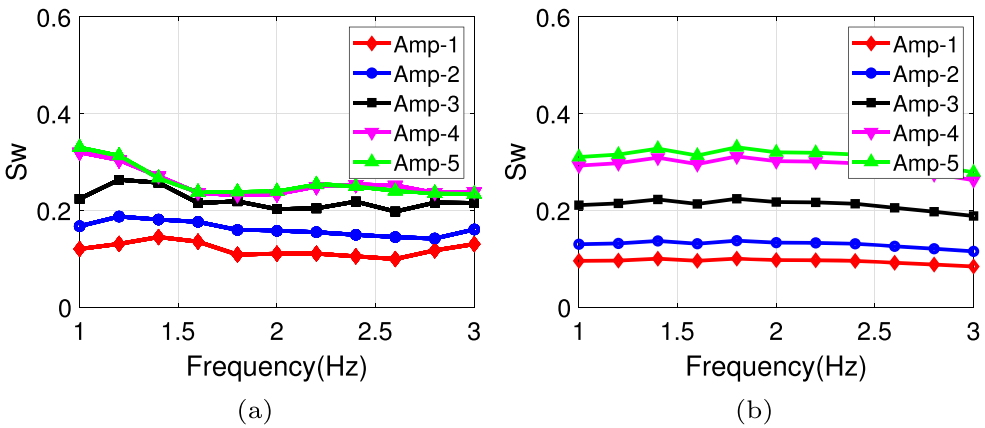

Fig. 10 The (a) experimental and (b) simulation curve of swimming number (Sw) under different Amplitudes; $Amp-i(i=1-5)$ represent the amplitudes of {4, 4.5, 6.5, 8, 9} cm, respectively

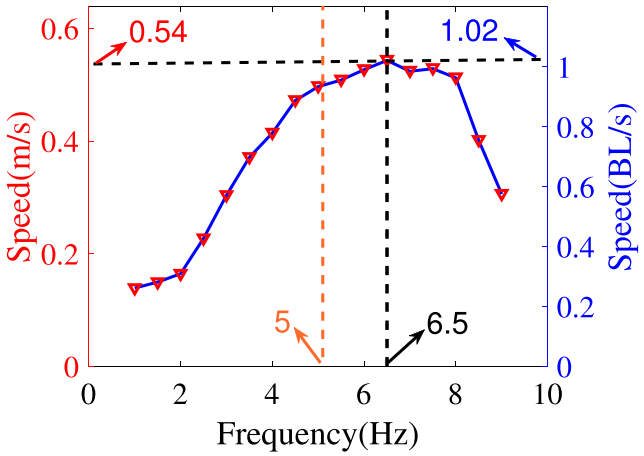

Fig. 11 The curve for swimming speed and frequency, where swing amplitude is 5 cm

- Our wire-driven elastic robotic fish achieves the maximum swimming speed of about 0.54 m/s, i.e., 1.02 BL/s, which is better than most of the existing wire-driven robot fish.

6 Conclusions and Future Works

This paper proposes a wire-driven elastic robotic fish, which simulates fish muscle through multi-wire drive and adopts a fishlike spine design based on elastic component. Remarkably, our robotic fish can realize the compliant simulation of fishlike swimming gait due to its distinctive designs, so it has the advantages of simple structure, easy control and good flexibility. More importantly, our robotic fish owns the continuous body wave, which improve its bionic degree. Besides, based on the arc assumption, the kinematics model and speed estimation model are derived, and PSO is adopted to determine CPG parameters so as to follow the fishlike swimming gait. Simulations and experiments demonstrate that our wire-driven elastic fishtail can serve as an efficient fishtail-like propeller and our robotic fish based on the proposed wire-driven elastic fishtail-like propeller not only achieves stable swimming, but also is capable of maximum average swimming speed of about 0.54 m/s, i.e., 1.02 BL/s.

In the future, we will explore the effect of the elastic spine on the motion performance, and further optimize swimming speed to obtain optimal parameters of body wave by speed estimation model. In addition, we will equip a variety of sensors for our robotic fish to perceive the environments, so as to avoid obstacles and so on. In short, there are still many difficulties for us to solve.

Table 2 Comparisons with existing wire-driven robotic fish

Robotic fish	Maximum Speed (BL/s)	Body Length (mm)
Li's wire-driven robotic fish [5]	0.35	425
Lau's wire-driven robotic fish [6]	0.22	600
Liu's continuum robotic dolphin [30]	0.44	817
Zhong's wire-driven robotic fish [31]	0.66	555
Zhong's wire-driven robotic fish [4]	2.15	310
Our wire-driven elastic robotic fish	1.02	530

Author Contributions Chao Zhou designed this study. Xiaocun Liao implemented the algorithms and performed the testing experiments. All authors, including Xiaocun Liao, Chao Zhou, Jian Wang, Junfeng Fan and Zhuoliang Zhang, contributed to the writing of the manuscript, and approved the final manuscript.

Funding This work was supported by National Nature Science Foundation of China (Grant numbers: 62033013, 61903362, 62003341, 61973303).

Data and code availability All data and code generated during and analysed during the current study are available from the corresponding author on reasonable request.

Declarations

Competing interests The authors have no relevant financial or non-financial interests to disclose.

References

1. Du, R., Li, Z., Youcef-Toumi, K., Alvarado, P.V. (eds.): Robot Fish: Bio-inspired Fishlike Underwater Robots. Springer, Germany (2015)
2. Scaradozzi, D., Palmieri, G., Costa, D., Pinelli, A.: BCF Swimming locomotion for autonomous underwater robots: a review and a novel solution to improve control and efficiency. Ocean Eng. **130**, 437–453 (2017)
3. Estarki, M., Varnousfaderani, R.H., Ghafarirad, H., Zareinejad, M.: Design and Implementation of a Soft Robotic Fish Based on Carangiform Fish Swimming. In: 2021 9Th RSI International Conference on Robotics and Mechatronics (ICRom). pp. 322-328, IEEE, Tehran, Iran, Republic of Islamic (2021)
4. Zhong, Y., Li, Z., Du, R.: A novel robot fish with wire-driven active body and compliant tail. IEEE/ASME Trans. Mechatron. **22**(4), 1633–1643 (2017)
5. Li, Z., Zhong, Y., Du, R.: A novel underactuated wire-driven robot fish with vector propulsion. In: 2013 IEEE/RSJ International Conference on Intelligent Robots and Systems, pp. 941-946, IEEE, Tokyo (2013)
6. Lau, W.P., Zhong, Y., Du, R., Li, Z.: Bladderless swaying wire-driven robot shark. In: 2015 IEEE 7Th International Conference on Cybernetics and Intelligent Systems (CIS) and IEEE Conference on Robotics, Automation and Mechatronics (RAM), pp. 155-160. IEEE, Siem Reap, Cambodia (2015)
7. Marcheseandrew, D., Onalcagdas, D.: Autonomous soft robotic fish capable of escape maneuvers using fluidic elastomer actuators. Soft Rob. **1**(1), 75–87 (2014)

8. Aubin, C.A., Choudhury, S., Jerch, R., Archer, L.A., Pikul, J.H., Shepherd, R.F.: Electrolytic vascular systems for energy-dense robots. Nature **571**(7763), 51–57 (2019)
9. Li, G., Chen, X., Zhou, F., Liang, Y., Xiao, Y., Cao, X., Yang, W.: Self-powered soft robot in the Mariana Trench. Nature **591**(7848), 66–71 (2021)
10. Liu, J., Hu, H.: Biological inspiration: from carangiform fish to multi-joint robotic fish. J. Bionic Eng. **7**(1), 35–48 (2010)
11. Wang, C., Xie, G., Wang, L., Cao, M.: CPG-Based locomotion control of a robotic fish: Using linear oscillators and reducing control parameters via PSO. International Journal of Innovative Computing Information and Control **7**(7B), 4237–4249 (2011)
12. Yang, W., Wu, P., Zhou, X., Zhu, P., Liu, X.: Central Pattern Generator Model Design and Gait Control Research of Amphibious Robotic Fish. J. Phys: Conf. Ser. **2029**(1), 012109 (2021)
13. Cao, Y., Ma, S., Xie, Y., Hao, Y., Zhang, D., He, Y., Cao, Y.: Parameter optimization of CPG network based on PSO for manta ray robot. In: Wu, M., Niu, Y., Gu, M., Cheng, J. (eds.) Proceedings of 2021 International Conference on Autonomous Unmanned Systems (ICAUS 2021), pp. 3062-3072, Springer, Singapore (2022)
14. Wang, W., Xie, G., Shi, H.: Dynamic Modeling of an Ostraciiform Robotic Fish Based on Angle of Attack Theory. In: 2014 International Joint Conference on Neural Networks (IJCNN), pp. 3944-3949, IEEE, Beijing (2014)
15. Zhang, Y., Li, Z., Du, Y.: Closed-Loop Pitch Attitude Control of Biomimetic Robotic Fish. In: 2020 IEEE 9Th Data Driven Control and Learning Systems Conference (DDCLS), pp 1193-1197, IEEE, Liuzhou, China (2020)
16. Jeong, I.-B., Park, C.-S., Na, K.-I., Han, S., Kim, J.-H.: Particle Swarm Optimization-Based Central Patter Generator for Robotic Fish Locomotion. In: 2011 IEEE Congress of Evolutionary Computation (CEC), pp. 152-157, IEEE, New Orleans, LA, USA (2011)
17. Kennedy, J., Eberhart, R.: Particle swarm optimization. In: Proceedings of ICNN'95 - International Conference on Neural Networks, pp. 1942-1948, IEEE, Perth, WA, Australia (1995)
18. Wang, M., Li, X., Dong, H., Yang, S.: A PSO-Based CPG Model Parameter Optimization Method for Biomimetic Robotic Fish. In: 2017 Chinese Automation Congress (CAC), pp. 3445-3449. IEEE, Jinan (2017)
19. Wang, M., Dong, H., Li, X., Zhang, Y., Yu, J.: Control and optimization of a bionic robotic fish through a combination of CPG model and PSO. Neurocomputing **337**, 144–152 (2019)
20. Yuan, J., Yu, J., Wu, Z., Tan, M.: Enhancing Swimming Performance of a Biomimetic Robotic Fish by Optimizing Oscillator Phase Differences of a CPG Model. In: 2015 IEEE International Conference on Robotics and Biomimetics (ROBIO), pp. 279-284. IEEE, Zhuhai, China (2015)
21. Crespi, A., Ijspeert, A.J.: Online optimization of swimming and crawling in an amphibious snake robot. IEEE Trans. Robot. **24**, 75–87 (2008)
22. Zhou, C., Low, K.H.: On-line optimization of biomimetic undulatory swimming by an experiment-based approach. J Bionic Eng. **11**, 213–225 (2014)
23. Tong, R., Qiu, C., Wu, Z., Wang, J., Tan, M., Yu, J.: Na-CPG: A robust and stable rhythm generator for robot motion control. Biomimetic Intelligence and Robotics, 100075 (2022)
24. Liao, X., Fu, Y., Lu, B., Zou, Q., Zhang, Z., Zhou, C.: An elastic biomimetic fish tail and its undulation fitting method of body wave. In: Proc. IEEE International Conference on Mechatronics and Automation (ICMA). pp. 1219-1225. IEEE, Takamatsu, Japan (2021)
25. Chen, D., Wu, Z., Dong, H., Tan, M., Yu, J.: Exploration of swimming performance for a biomimetic multi-joint robotic fish with a compliant passive joint. Bioinspir. Biomim. **16**(2), 026007 (2020)
26. Ijspeert, A.J., Crespi, A., Ryczko, D., Cabelguen, J.M.: From swimming to walking with a salamander robot driven by a spinal cord model. Science. **315**(5817), 1416–1420 (2007)
27. Lighthill, M.J.: Note on the swimming of slender fish. J Fluid Mech **9**(2), 305–317 (1960)
28. Valdivia, Y., Alvarado, P., Youcef-Toumi, K.: Design of machines with compliant bodies for biomimetic locomotion in liquid environments. Trans ASME J Dyn Syst Meas Control **128**(1), 3–13 (2006)
29. Zhao, W., Ming, A., Shimojo, M.: Development of high-performance soft robotic fish by numerical coupling analysis. Applied Bionics and Biomechanics, 2018 (2018)
30. Liu, J., Zhang, C., Liu, Z., Zhao, R., An, D., Wei, Y., Yu, J.: Design and analysis of a novel tendon-driven continuum robotic dolphin. Bioinspir. Biomim. **16**(6), 065002 (2021)
31. Zhong, Y., Li, Z., Du, R.: The Design and Prototyping of a Wire-Driven Robot Fish with Pectoral Fins. In: 2013 IEEE International Conference on Robotics and Biomimetics (ROBIO). pp. 1918-1923. IEEE, Shenzhen, China (2013)

Xiaocun Liao received the B.E. degree in Detection, Guidance and Control Technology from Central South University (CSU), Changsha, China, in 2019. He is currently working toward the Ph.D. degree in control theory and control engineering with the Institute of Automation, Chinese Academy of Sciences (IACAS), Beijing, China. His research interests include the bioinspired robot fish and intelligent control systems.

Chao Zhou received the B.E. degree in automation from Southeast University, Nanjing, China, in July 2003, and the Ph.D. degree in control theory and control engineering from the Institute of Automation, Chinese Academy of Sciences (IACAS), Beijing, China, in 2008. He is currently a Professor with the State Key Laboratory of Management and Control for Complex Systems, IACAS. His current research interests include the motion control of robot, the bioinspired robotic fish, and embedded system of robot.

Jian Wang received the B.E. degree in automation from the University of Science and Technology Beijing, Beijing, China, in 2016, and the Ph.D. degree in control theory and control engineering from the Institute of Automation, Chinese Academy of Sciences (IACAS), Beijing,China, in 2021. He is currently an Assistant Professor with the State Key Laboratory of Management and Control for Complex Systems, IACAS. His research interests include bioinspired underwater robots and intelligent control systems.

Junfeng Fan received the B.S. degree in mechanical engineering and automation from Beijing Institute of Technology, Beijing, China, in 2014 and Ph.D. degree in control theory and control engineering from the Institute of Automation, Chinese Academy of Sciences (IACAS), Beijing, China, in 2019. He is currently an Associate Professor of Control Theory and Control Engineering with the State Key Laboratory of Management and Control for Complex Systems, IACAS, Beijing. His research interests include robot vision and underwater robot.

Zhuoliang Zhang received the B.E. degree in automation from Tongji University, Shanghai, China, in July 2018. He is currently pursuing the Ph.D. degree in control theory and control engineering with the Institute of Automation, Chinese Academy of Sciences, and also with the University of Chinese Academy of Sciences, Beijing. His research interests include measurements, sensor signal processing, and intelligent control.

Terms and Conditions

Springer Nature journal content, brought to you courtesy of Springer Nature Customer Service Center GmbH (“Springer Nature”).
Springer Nature supports a reasonable amount of sharing of research papers by authors, subscribers and authorised users (“Users”), for small-scale personal, non-commercial use provided that all copyright, trade and service marks and other proprietary notices are maintained. By accessing, sharing, receiving or otherwise using the Springer Nature journal content you agree to these terms of use (“Terms”). For these purposes, Springer Nature considers academic use (by researchers and students) to be non-commercial.
These Terms are supplementary and will apply in addition to any applicable website terms and conditions, a relevant site licence or a personal subscription. These Terms will prevail over any conflict or ambiguity with regards to the relevant terms, a site licence or a personal subscription (to the extent of the conflict or ambiguity only). For Creative Commons-licensed articles, the terms of the Creative Commons license used will apply.
We collect and use personal data to provide access to the Springer Nature journal content. We may also use these personal data internally within ResearchGate and Springer Nature and as agreed share it, in an anonymised way, for purposes of tracking, analysis and reporting. We will not otherwise disclose your personal data outside the ResearchGate or the Springer Nature group of companies unless we have your permission as detailed in the Privacy Policy.
While Users may use the Springer Nature journal content for small scale, personal non-commercial use, it is important to note that Users may not:

1. use such content for the purpose of providing other users with access on a regular or large scale basis or as a means to circumvent access control;
2. use such content where to do so would be considered a criminal or statutory offence in any jurisdiction, or gives rise to civil liability, or is otherwise unlawful;
3. falsely or misleadingly imply or suggest endorsement, approval , sponsorship, or association unless explicitly agreed to by Springer Nature in writing;
4. use bots or other automated methods to access the content or redirect messages
5. override any security feature or exclusionary protocol; or
6. share the content in order to create substitute for Springer Nature products or services or a systematic database of Springer Nature journal content.

In line with the restriction against commercial use, Springer Nature does not permit the creation of a product or service that creates revenue, royalties, rent or income from our content or its inclusion as part of a paid for service or for other commercial gain. Springer Nature journal content cannot be used for inter-library loans and librarians may not upload Springer Nature journal content on a large scale into their, or any other, institutional repository.
These terms of use are reviewed regularly and may be amended at any time. Springer Nature is not obligated to publish any information or content on this website and may remove it or features or functionality at our sole discretion, at any time with or without notice. Springer Nature may revoke this licence to you at any time and remove access to any copies of the Springer Nature journal content which have been saved.
To the fullest extent permitted by law, Springer Nature makes no warranties, representations or guarantees to Users, either express or implied with respect to the Springer nature journal content and all parties disclaim and waive any implied warranties or warranties imposed by law, including merchantability or fitness for any particular purpose.
Please note that these rights do not automatically extend to content, data or other material published by Springer Nature that may be licensed from third parties.
If you would like to use or distribute our Springer Nature journal content to a wider audience or on a regular basis or in any other manner not expressly permitted by these Terms, please contact Springer Nature at

onlineservice@springernature.com